Orchestration of the DNA-Damage Response by the RNF8 Ubiquitin Ligase
Nadine K. Kolas, *et al.*
Science **318**, 1637 (2007);
DOI: 10.1126/science.1150034

Orchestration of the DNA-Damage Response by the RNF8 Ubiquitin Ligase

Nadine K. Kolas,[1]* J. Ross Chapman,[2]* Shinichiro Nakada,[1]* Jarkko Ylanko,[1,3] Richard Chahwan,[2] Frédéric D. Sweeney,[1,3] Stephanie Panier,[1] Megan Mendez,[1] Jan Wildenhain,[1] Timothy M. Thomson,[4] Laurence Pelletier,[1,3] Stephen P. Jackson,[2]† Daniel Durocher[1,3]†

Cells respond to DNA double-strand breaks by recruiting factors such as the DNA-damage mediator protein MDC1, the p53-binding protein 1 (53BP1), and the breast cancer susceptibility protein BRCA1 to sites of damaged DNA. Here, we reveal that the ubiquitin ligase RNF8 mediates ubiquitin conjugation and 53BP1 and BRCA1 focal accumulation at sites of DNA lesions. Moreover, we establish that MDC1 recruits RNF8 through phosphodependent interactions between the RNF8 forkhead-associated domain and motifs in MDC1 that are phosphorylated by the DNA-damage activated protein kinase ataxia telangiectasia mutated (ATM). We also show that depletion of the E2 enzyme UBC13 impairs 53BP1 recruitment to sites of damage, which suggests that it cooperates with RNF8. Finally, we reveal that RNF8 promotes the G_2/M DNA damage checkpoint and resistance to ionizing radiation. These results demonstrate how the DNA-damage response is orchestrated by ATM-dependent phosphorylation of MDC1 and RNF8-mediated ubiquitination.

DNA double-strand breaks (DSBs) are highly cytotoxic lesions, and to ensure that they are repaired with minimal impact on genome stability, cells mount a complex DNA-damage response (DDR) that includes the spatial reorganization of DSB repair and signaling proteins into subnuclear structures—ionizing radiation–induced foci (IRIF)—that surround DSB sites (*1*, *2*). Most IRIF formation depends on phosphorylation of the histone variant H2AX (to form γH2AX) by the DNA-dependent and ataxia telangiectasia mutated (ATM) protein kinases (*3*–*6*). The γH2AX epitope is bound by MDC1 (*7*–*10*) that then promotes IRIF formation by other proteins, including 53BP1, Nijmegen-breakage-syndrome protein NBS1, and BRCA1 (*11*, *12*). BRCA1 recruitment to IRIF requires

[1]Samuel Lunenfeld Research Institute, Mount Sinai Hospital, 600 University Avenue, Toronto M5G 1X5, Ontario, Canada. [2]The Wellcome Trust and Cancer Research UK Gurdon Institute, and the Department of Zoology, University of Cambridge, Tennis Court Road, Cambridge CB2 1QN, UK. [3]Department of Molecular Genetics, University of Toronto, Toronto, Ontario, Canada. [4]Department of Molecular and Cellular Biology, Instituto de Biología Molecular de Barcelona calle Jordi Girona 18-26, 08034 Barcelona, Spain.

*These authors contributed equally to this work.
†To whom correspondence should be addressed. E-mail: durocher@mshri.on.ca (D.D.); s.jackson@gurdon.cam.ac.uk (S.P.J.)

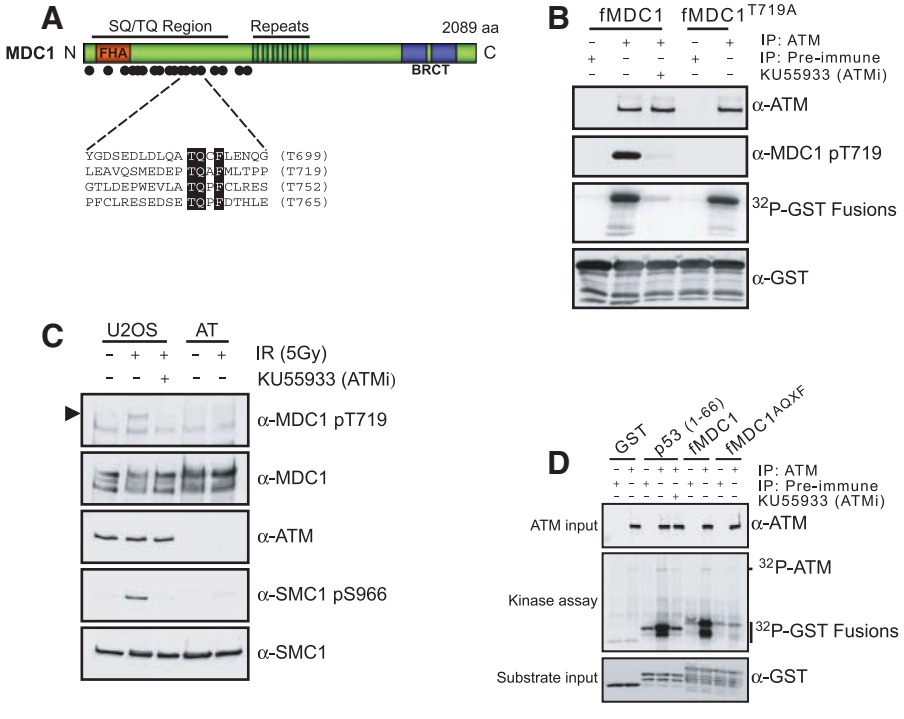

Fig. 1. The MDC1 TQXF motifs are ATM targets required for 53BP1 IRIF. (**A**) Domain architecture of MDC1, with ATM consensus sites (dots). (**B**) MDC1 T719 is phosphorylated by ATM in vitro. GST-MDC1$^{679\text{-}778}$ (fMDC1) or GST-MDC1$^{679\text{-}778\text{-}T719A}$ (fMDC1^{T719A}) were incubated with antibody to ATM or preimmune complexes in the presence or absence of the ATM kinase inhibitor KU55933. (**C**) MDC1 TQXF motifs are phosphorylated by ATM in vivo. Lysates from U2OS or AT22IJE (AT) cells were immunoblotted with the indicated antibodies. The arrowhead points to phospho-MDC1. (**D**) The MDC1 TQXF motifs are phosphorylated by ATM in vitro. Kinase reactions with antibody to ATM or preimmune complexes and the following substrates: GST, GST-p53$^{1\text{-}66}$ [p53(1-66)], fMDC1 or GST-MDC1$^{679\text{-}778\text{-}AQXF}$ (fMDC1^{AQXF}), as in (B). (**E** and **F**) The TQXF cluster is required for 53BP1 IRIF. U2OS cells expressing siRNA-resistant GFP-MDC1 (MDC1*) or GFP-MDC1^{AQXF} (MDC1^{*AQXF}) were transfected with siRNA against MDC1 (siMDC1) or luciferase (siCTRL), and after irradiation (5 Gy) were stained for MDC1 and 53BP1 (E) and quantitated (F) (N = 4 ± SD).

its interaction with the ubiquitin-binding protein RAP80 (*13*–*16*) that interacts with lysine 63 (K63)–linked polyubiquitinated protein(s) at sites of DNA damage (*15*). Here, we identify RNF8 as the prime ubiquitin ligase for ubiquitination at DSB sites, define its functional importance in the DDR, and establish how RNF8 is recruited to sites of DNA damage through interactions with MDC1.

MDC1 is phosphorylated in an ATM-dependent manner in response to ionizing radiation (IR) (*11*, *12*). Potential ATM target sites (consensus S/T-Q) cluster in the MDC1 N terminus, the most notable being four adjacent motifs conforming to the consensus TQXF (Fig. 1A and fig. S1). Notably, antibodies raised against a peptide encoding phospho-T719 (fig. S2A) indicated that it is targeted by ATM in vitro (Fig. 1B) and in vivo (Fig. 1C and fig. S2B). However, in vitro assays with bacterially expressed MDC1 fragments revealed that T719 was not the only site of ATM modification. Phosphorylation was only abolished when an "AQXF" mutant protein bearing threonine-to-alanine substitutions in all four TQXF motifs was used as substrate (Fig. 1D). These data and the recent identification of another TQXF site (T752) as an ATM target (*17*) therefore imply that MDC1 TQXF motifs are likely all modified by ATM and may function redundantly with one another.

To address the function of the MDC1 TQXF motifs, we used small interfering RNA (siRNA) to deplete endogenous MDC1 in human U2OS cells stably expressing siRNA-resistant wild-type MDC1 or the MDC1 AQXF mutant. Although both wild-type and AQXF mutant proteins formed IRIF and supported IRIF formation by NBS1 (fig. S3), only wild-type MDC1 promoted effective IRIF formation by 53BP1 (Fig. 1, E and F), revealing that ATM-mediated phosphorylation of MDC1 facilitates 53BP1 focus formation. Indeed, although 53BP1 IRIF formation can occur in ATM-deficient AT cells (*18*, *19*), we found that pharmacological inhibition of ATM impaired 53BP1 focus formation (fig. S4). Although these results suggested that 53BP1 might directly bind the phosphorylated TQXF motifs, we were unable to detect such interactions, which suggests that MDC1-dependent 53BP1 IRIF formation is likely mediated by an additional factor.

To uncover proteins that regulate 53BP1 focus formation, we mined an ongoing RNA interference (RNAi) screen that employs 53BP1 focus formation as a readout (Fig. 2A and fig. S5, A to C). Notably, the three siRNAs that most potently impaired 53BP1 focus formation targeted transcripts encoding MDC1, ubiquitin, and the RNF8 E3 ubiquitin ligase that was recently shown to control mitosis (*20*) (Fig. 2A). Notably, we found that depletion of RNF8 by siRNA or enzyme-generated siRNA pools (esiRNAs) (*21*) abrogated 53BP1 foci while preserving MDC1 IRIF, thus phenocopying the $MDC1^{AQXF}$ mutation (Fig. 2, B and C, and fig. S6A). Introduction of RNAi-resistant murine RNF8 into cells transfected with RNF8 siRNA restored 53BP1 focus formation (Fig. 2D and fig. S7), indicating the specificity of RNF8 depletion and confirming that RNF8 promotes 53BP1 IRIF formation.

RNF8 possesses an N-terminal forkhead-associated (FHA) domain (*22*) and a C-terminal RING-finger domain responsible for its ubiquitin ligase activity (Fig. 2E) (*23*). By complementing the human RNF8 RNAi phenotype with siRNA-resistant murine RNF8, we established that mutations in either the FHA domain ($RNF8^{R42A}$) or RING-finger domain ($RNF8^{C406S}$) abrogated the ability of RNF8 to support 53BP1 IRIF formation (Fig. 2, E and F, and fig. S7). As FHA domains bind phosphothreonine-bearing epitopes, the above data suggested that RNF8 might interact with ATM-phosphorylated MDC1. Indeed, the RNF8 FHA domain, but not an FHA-domain mutant ($RNF8^{R42A}$), bound specifically and in a phospho-dependent manner to TQXF peptides corresponding to MDC1 Thr719 or Thr752 (Fig. 3A). Furthermore, these phosphorylated TQXF peptides retrieved RNF8 from HeLa nuclear extracts, whereas the corresponding unphosphorylated peptides did not (Fig. 3B). Notably, epitope-tagged RNF8, but not $RNF8^{R42A}$, was detected in MDC1 immunoprecipitates in a manner that was enhanced by irradiation (Fig. 3C), which suggests that MDC1 might recruit RNF8 to sites of DNA damage. To test this idea, we generated cell lines stably expressing RNF8 fused to yellow fluorescent protein (YFP). As shown by analysis of live cells (Fig. 3D) and fixed samples (fig. S8), addition of the radio-mimetic drug phleomycin or

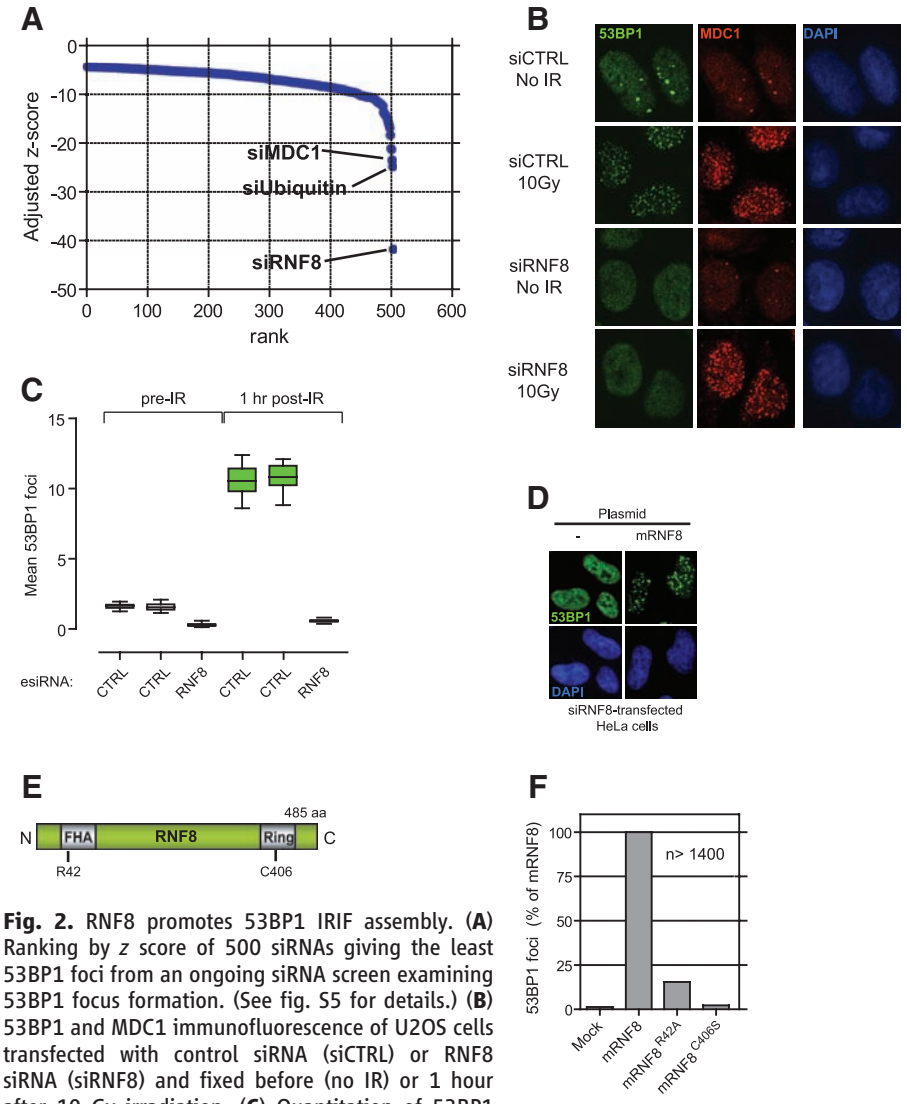

Fig. 2. RNF8 promotes 53BP1 IRIF assembly. (**A**) Ranking by *z* score of 500 siRNAs giving the least 53BP1 foci from an ongoing siRNA screen examining 53BP1 focus formation. (See fig. S5 for details.) (**B**) 53BP1 and MDC1 immunofluorescence of U2OS cells transfected with control siRNA (siCTRL) or RNF8 siRNA (siRNF8) and fixed before (no IR) or 1 hour after 10 Gy irradiation. (**C**) Quantitation of 53BP1 IRIF in HeLa cells transfected with the indicated esiRNAs (CTRL against luciferase). $N = 16$, data displayed using box-and-whisker plots. (**D**) Transfection of siRNA-resistant murine *RNF8* in HeLa cells restores 53BP1 IRIF formation caused by RNF8 depletion. (**E**) Domain architecture of RNF8. Numbering refers to murine RNF8. (**F**) Rescue of RNF8 depletion by murine RNF8 but not the FHA-(R42A) or RING finger–mutated (C406s) mutants. 53BP1 foci were quantitated 1 hour after 10 Gy irradiation in siRNF8-treated cells. Data for wild-type RNF8 were set at 100%. More than 1400 cells per condition were counted.

irradiation resulted in the accumulation of YFP-RNF8 into foci that colocalized with γH2AX. In support of such events being brought about by ATM-mediated phosphorylation of MDC1, YFP-RNF8 recruitment was impaired by the selective ATM inhibitor KU55933 (*24*) (Fig. 3D).

As was the case for MDC1 foci, we found that γH2AX, NBS1, and FANCD2 foci formed efficiently in RNF8-depleted cells (fig. S9). In contrast, BRCA1 IRIF formation was impaired upon RNF8 depletion (Fig. 3E). BRCA1-interacting protein RAP80 is required for BRCA1 IRIF formation (*13*–*16*), and RAP80 itself forms IRIF in a manner that involves interactions between its ubiquitin-interacting motif (UIM) and K63-linked ubiquitin chains at sites of DNA lesions (*13*–*16*). Because RNF8 is a ubiquitin ligase that promotes BRCA1 IRIF, we speculated that RNF8 might

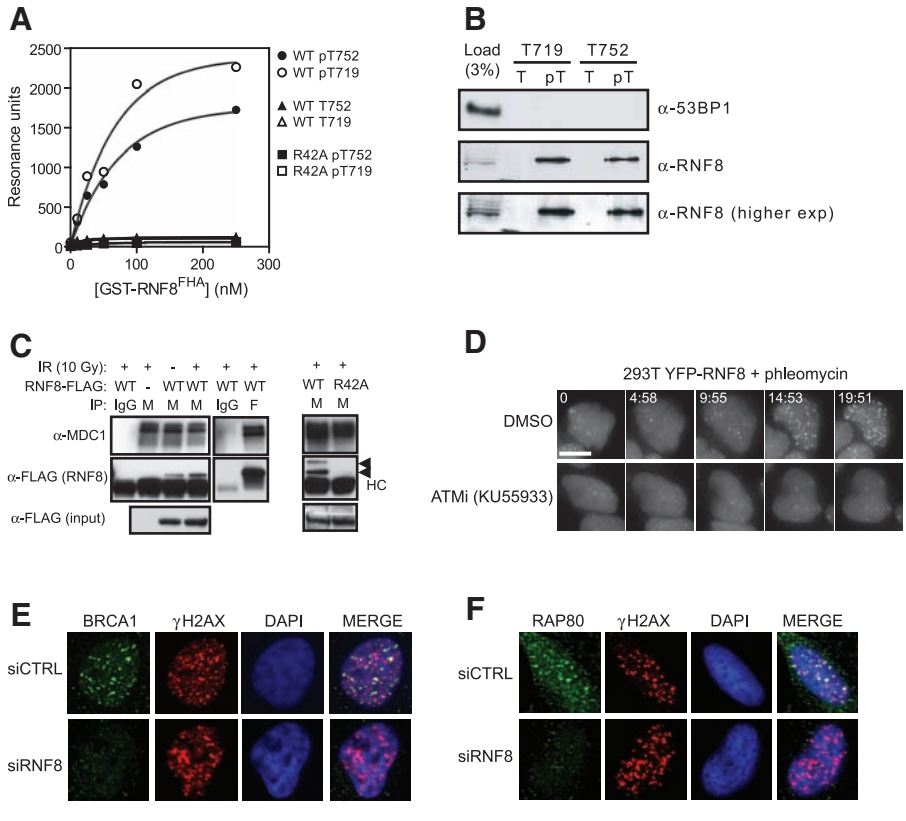

Fig. 3. RNF8 mediates BRCA1-RAP80 IRIF through a physical interaction with MDC1. (**A**) Binding curves of GST-RNF8^{FHA} (WT), the R42A mutant obtained by surface plasmon resonance with peptides corresponding to MDC1 epitopes surrounding T719, T752, or their phosphorylated counterparts (pT719 and pT752). (**B**) Peptide pull-downs of HeLa nuclear extracts with immobilized peptides; phosphorylated (pT) or unphosphorylated (T), encompassing MDC1 T719 or T752 residues. (**C**) RNF8 interacts with MDC1 in vivo. Extracts from 293T cells mock-transfected (–) or transfected (+) with RNF8-FLAG (WT) or the R42A FHA mutant were immunoprecipitated (IP) with antibodies to MDC1 (M), FLAG (F), or normal mouse immunoglobulin G (IgG) and probed for MDC1 or RNF8-FLAG as indicated. Arrowheads indicate the RNF8-specific signal. RNF8 appears modified when interacting with MDC1. HC, IgG heavy chains. (**D**) Time-lapse microscopy of 293T cells stably expressing YFP-RNF8 preincubated with ATM inhibitor KU55933 or dimethyl sulfoxide and treated with the radio-mimetic drug phleomycin (1.5 mg/ml) for the indicated times (min:sec). Three-dimensional (3D) image data sets were computationally deconvolved and shown as 2D projections. Scale bar, 10 μm. (**E** and **F**) Irradiated (10 Gy) HeLa cells transfected with the indicated siRNAs were stained with antibodies to γH2AX, BRCA1 (D), or RAP80 (E) 1 hour after IR.

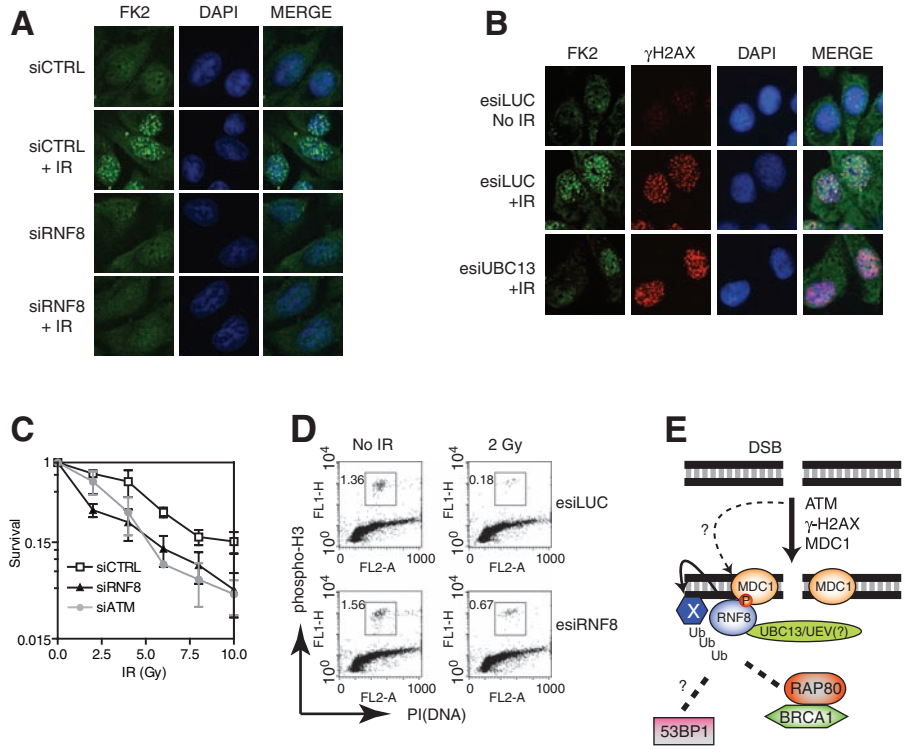

Fig. 4. RNF8 cooperates with UBC13 to mediate ubiquitin IRIF and a functional DDR. (**A** and **B**) Irradiated (10 Gy) U2OS cells transfected with the indicated siRNA (A) or esiRNAs (B) were stained with FK2 antibodies to conjugated ubiquitin and γH2AX to assess IRIF. Cells were fixed 1 hour after IR. (**C**) Clonogenic survival of HeLa cells transfected with siRNAs against ATM (siATM), RNF8 (siRNF8), or a non-targeting control (siCTRL). $N = 3 \pm$ SEM. (**D**) G_2/M checkpoint analysis of U2OS cells transfected with the indicated esiRNAs. Fixed mock-treated (No IR) or irradiated (2 Gy) cells were stained with an antibody to phospho-histone H3 and propidium iodide (PI). The percentage of mitotic cells was determined by fluorescence-activated cell sorting. (**E**) Model of RNF8 action at DSBs. RNF8 is recruited by ATM-phosphorylated MDC1 to DSBs, where it ubiquitinates an unknown protein (X), recruiting RAP80-BRCA1 and allowing 53BP1 to recognize methylated histones, as suggested by the RNF8-dependent recruitment of the 53BP1 Tudor domain to DSB sites (fig. S13). Our results also suggest the presence of a MDC1-independent pathway of RNF8 action (dashed line) that mediates 53BP1 and BRCA1 IRIF formation.

mediate IRIF formation by RAP80 and conjugated ubiquitin. Indeed, RNF8 was essential for IRIF formation in both cases (Figs. 3F and 4A, and fig. S10A). Because RAP80 is not required for 53BP1 focus formation after IR (*14*) and 53BP1 is not needed for RAP80 IRIF (fig. S10B), these results indicated that RNF8 acts downstream of MDC1 to promote at least two types of IRIF: those containing 53BP1 and those containing BRCA1. In support of this model, mutation of the TQXF motifs in MDC1 also impaired BRCA1 and conjugated ubiquitin IRIF (fig. S11).

RNF8 can bind to multiple E2-conjugating enzymes to catalyze both K63-linked and K48-linked ubiquitin chains (*23*, *25*). When we screened a panel of 13 E2 enzymes by RNAi and quantitative microscopy, only UBC13 depletion markedly impaired 53BP1 IRIF formation (fig. S12). UBC13 depletion also impaired IRIF by conjugated ubiquitin (Fig. 4B). Entirely consistent with our data, genetic ablation of UBC13 in DT40 cells abrogate BRCA1 and ubiquitin IRIF (*26*). As UBC13 is the only known E2-conjugating enzyme that catalyzes K63-linked polyubiquitination, these findings are consistent with data indicating that ubiquitin IRIF form in part through K63-linked polyubiquitination (*15*, *26*). Moreover, as UBC13 physically interacts with RNF8 to catalyze K63-linked ubiquitin chains (*27*), the available data imply that RNF8 is responsible for formation of K63-linked ubiquitin chains at DSB sites.

Consistent with RNF8 playing an important function in the DDR, we found that RNF8 depletion caused IR hypersensitivity in clonogenic cell-survival assays (Fig. 4C). Furthermore, a greater proportion of RNF8-depleted cells progressed into M phase after irradiation than did cells transfected with a control esiRNA, which indicates that RNF8 enforces the G_2/M DNA-damage checkpoint (Fig. 4D).

Our results identify mammalian RNF8 as an important component of the DDR. Specifically, RNF8 binds to ATM-target motifs on MDC1, thus recruiting RNF8 to DSB sites. RNF8 then triggers the formation of ubiquitin conjugates that promote recruitment of the RAP80-BRCA1 complex and 53BP1 to DSB sites, thereby enhancing DNA-damage checkpoint events and promoting cell survival (Fig. 4E).

References and Notes

1. J. Bartek, J. Lukas, *Curr. Opin. Cell Biol.* **19**, 238 (2007).
2. R. S. Maser, K. J. Monsen, B. E. Nelms, J. H. Petrini, *Mol. Cell. Biol.* **17**, 6087 (1997).
3. T. Stiff *et al.*, *Cancer Res.* **64**, 2390 (2004).
4. T. T. Paull *et al.*, *Curr. Biol.* **10**, 886 (2000).
5. A. Celeste *et al.*, *Nat. Cell Biol.* **5**, 675 (2003).
6. S. Bekker-Jensen *et al.*, *J. Cell Biol.* **173**, 195 (2006).
7. M. Stucki *et al.*, *Cell* **123**, 1213 (2005).
8. Z. Lou *et al.*, *Mol. Cell* **21**, 187 (2006).
9. M. S. Lee, R. A. Edwards, G. L. Thede, J. N. Glover, *J. Biol. Chem.* **280**, 32053 (2005).
10. S. Bekker-Jensen, C. Lukas, F. Melander, J. Bartek, J. Lukas, *J. Cell Biol.* **170**, 201 (2005).
11. G. S. Stewart, B. Wang, C. R. Bignell, A. M. Taylor, S. J. Elledge, *Nature* **421**, 961 (2003).
12. M. Goldberg *et al.*, *Nature* **421**, 952 (2003).
13. J. Yan *et al.*, *Cancer Res.* **67**, 6647 (2007).
14. H. Kim, J. Chen, X. Yu, *Science* **316**, 1202 (2007).
15. B. Sobhian *et al.*, *Science* **316**, 1198 (2007).
16. B. Wang *et al.*, *Science* **316**, 1194 (2007).
17. S. Matsuoka *et al.*, *Science* **316**, 1160 (2007).
18. R. A. DiTullio Jr. *et al.*, *Nat. Cell Biol.* **4**, 998 (2002).
19. L. B. Schultz, N. H. Chehab, A. Malikzay, T. D. Halazonetis, *J. Cell Biol.* **151**, 1381 (2000).
20. V. Plans, M. Guerra-Rebollo, T. M. Thomson, *Oncogene*, in press. Published online 3 September 2007 (10.1038/sj.onc.1210782).
21. R. Kittler, A. K. Heninger, K. Franke, B. Habermann, F. Buchholz, *Nat. Methods* **2**, 779 (2005).
22. D. Durocher, J. Henckel, A. R. Fersht, S. P. Jackson, *Mol. Cell* **4**, 387 (1999).
23. K. Ito *et al.*, *Eur. J. Biochem.* **268**, 2725 (2001).
24. I. Hickson *et al.*, *Cancer Res.* **64**, 9152 (2004).
25. J. Bothos, M. K. Summers, M. Venere, D. M. Scolnick, T. D. Halazonetis, *Oncogene* **22**, 7101 (2003).
26. G. Y. Zhao *et al.*, *Mol. Cell* **25**, 663 (2007).
27. V. Plans *et al.*, *J. Cell. Biochem.* **97**, 572 (2006).

28. We thank members of the Durocher and Jackson laboratories for input on the manuscript and M. Vojvodic for experimental assistance. We also thank A. C. Gingras for the stable YFP-RNF8 line, KuDOS Pharmaceuticals for providing inhibitors and reagents, and Abcam for the MDC1 pT719 antibody. This work was supported by grants from the Canadian Institutes of Health Research (CIHR) to D.D. and by funding from Cancer Research UK and the European Union (S.P.J.). N.K.K. is a CIHR postdoctoral fellow and an alumnus of the Excellence in Radiation Research for the 21st Century training program; F.D.S. holds a Terry-Fox studentship from the National Cancer Institute of Canada; S.N. is a Gail-Posluns Fellow and is supported by the Mitsubishi Pharma Research Foundation. D.D. is a Canada Research Chair (Tier II) in Proteomics, Functional Genomics, and Bioinformatics.

Supporting Online Material

www.sciencemag.org/cgi/content/full/1150034/DC1
Materials and Methods
Figs. S1 to S14
References

4 September 2007; accepted 5 November 2007
Published online 15 November 2007;
10.1126/science.1150034
Include this information when citing this paper.

Engineering Modified Bt Toxins to Counter Insect Resistance

Mario Soberón,[1]* Liliana Pardo-López,[1] Idalia López,[1] Isabel Gómez,[1] Bruce E. Tabashnik,[2] Alejandra Bravo[1]*

The evolution of insect resistance threatens the effectiveness of *Bacillus thuringiensis* (Bt) toxins that are widely used in sprays and transgenic crops. Resistance to Bt toxins in some insects is linked with mutations that disrupt a toxin-binding cadherin protein. We show that susceptibility to the Bt toxin Cry1Ab was reduced by cadherin gene silencing with RNA interference in *Manduca sexta*, confirming cadherin's role in Bt toxicity. Native Cry1A toxins required cadherin to form oligomers, but modified Cry1A toxins lacking one α-helix did not. The modified toxins killed cadherin-silenced *M. sexta* and Bt-resistant *Pectinophora gossypiella* that had cadherin deletion mutations. Our findings suggest that cadherin promotes Bt toxicity by facilitating toxin oligomerization and demonstrate that the modified Bt toxins may be useful against pests resistant to standard Bt toxins.

The toxins produced by *Bacillus thuringiensis* (Bt) kill some major insect pests such as mosquitoes and crop-eating caterpillars but are harmless to vertebrates and most other organisms (*1*). Transgenic corn and cotton producing Bt toxins grew on more than 32 million hectares worldwide in 2006 (*2*). The primary threat to the long-term efficacy of Bt toxins is the evolution of resistance by pests (*3*–*5*). Many insects have been selected for resistance to Bt toxins in the laboratory, and two crop pests (*Plutella xylostella* and *Trichoplusia ni*) have evolved resistance to Bt sprays outside of the laboratory (*3*–*13*). The most widely used Bt toxins are crystal toxins in the Cry1A family, particularly Cry1Ab in transgenic Bt corn and Cry1Ac in transgenic Bt cotton, which kill caterpillars (lepidopteran larvae) (*7*). Cry1A toxins bind to the extracellular domain of cadherin proteins that traverse the insect larval midgut membrane (*14*). Disruption of Bt toxin binding to midgut receptors is the most common mechanism of insect resistance (*6*). Mutations in the midgut cadherins that bind Cry1Ac are linked with and probably cause resistance in at least three lepidopteran pests of cotton (*5*, *10*, *12*).

Two hypotheses proposed to explain how Cry1A toxins function are the pore-formation model and the signaling model (*15*, *16*). These theories share initial steps: Cry1A protoxins are ingested, solubilized in the gut, and cleaved by midgut proteases such as trypsin to yield activated 60-kD monomeric toxins that bind to cadherin with high affinity (*14*). The signaling model, derived from studies of insect cell cultures, suggests that after protease-activated monomeric toxins bind to cadherin, initiation of a magnesium-dependent signaling pathway causes cell death (*16*). In contrast, on the basis of results from in vitro experiments and bioassays, the pore-formation model proposes that protease-activated monomers bind to cadherin to facilitate protease cleavage of the N terminus of the toxin, including helix α-1of domain I (*17*, *18*). This cleavage induces the assembly of oligomeric forms of the toxin, which have increased binding affinity to secondary receptors,

[1]Instituto de Biotecnología, Universidad Nacional Autónoma de México, Apartado Postal 510-3, Cuernavaca 62250, Morelos, Mexico. [2]Department of Entomology, University of Arizona, Tucson, AZ, USA.

*To whom correspondence should be addressed. E-mail: bravo@ibt.unam.mx (A.B.); mario@ibt.unam.mx (M.S.)